This article has been accepted for publication in a future issue of this journal, but has not been fully edited. Content may change prior to final publication. Citation information: DOI 10.1109/OJAP.2020.2986001, IEEE Open Journal of Antennas and Propagation

Machine Learning Classification of S-Band Microwave Scattering Measurements from the Forearm as a Novel Biometric Technique

Ala-Addin Nabulsi, *Student Member, IEEE,* Waleed Al-Shaikhli, *Student Member, IEEE,* Clayton Kettlewell, *Student Member, IEEE,* Kyle Hejtmanek, *Student Member, IEEE,* Ahmed M. Hassan, *Senior Member, IEEE,* and Reza Derakhshani, Member, IEEE[1]

***Abstract*—Biometrics use an individual's biological traits for personal identification. Various sensors have been used to obtain these measurements. Microwave biometric scans have recently gained traction as a non-contact technique due to their robustness to environmental lighting and unobtrusiveness. To evaluate microwave signature of human forearm as a biometric modality, an 8-antenna (Wi-Fi) data collection setup was developed and initially tested with foil-wrapped tubes of different geometric cross sections. The system was later evaluated by collecting microwave samples from human volunteers' forearms and classifying the data, from different antenna subsets, using Support Vector Machines and Naive Bayesian classifiers. Our results show that human identification via microwave signals is possible even with a subset of the above mentioned 8-antenna configuration.**

***Index Terms*—Microwave Signals, Biometrics, Machine Learning, Wi-Fi.**

I. Introduction

Biometrics is the science of measurement and analysis of individuals' unique physical or behavioral characteristics in order to establish their identity. To date, numerous biometric systems have been developed for securing digital access to corporate and personal data, or for securing physical access to safes and buildings, to name a few. These systems have used a multitude of body measurements, including fingerprints, irises, faces, Eyeprints, palms, gait and voice [1]–[7]. These biometric measurements, for the majority, are collected by cameras. They do achieve very good results, but using cameras has certain disadvantages including occlusions and sensitivity to different lighting conditions, as well as various presentation attacks (spoofing) [8]. To make them more reliable, biometric systems need to improve not only their accuracy but more importantly their user experience and security. Microwave signals have been used for target scanning for many years. Certain microwave-based imaging systems can generate the kind of imagery that might be usable by image classification techniques. For example, Ostadrahimi *et al.* developed a Microwave Tomography (MWT) system that utilized a circular array of 24 antennas to reconstruct a cross-sectional image of the target located inside the antenna array [9]. In their work, the collected electric field data was used to reconstruct the dielectric properties of the object of interest. The Multiplicative Regularized Gauss-Newton Inversion (MR-GNI) algorithm was used to successfully reconstruct images from different objects, at a frequency of 4.5GHz.

Abo Rahama *et al.* developed MWT system that is quite unique compared to others [10]. Their system consisted of transmitting antenna array on one side and receiving antennas on the other three side of the imaging chamber. The transmitter array's phase configuration was change 31 times for each frequency used. Due to the complexity of the forward solver used for the inversion algorithm for this particular system setup, Artificial Neural Networks were used to develop the mathematical models used for the image reconstruction. Their system successfully reconstructed images of objects of interest at 3 frequencies: 3.2, 3.5, and 3.8 GHz. The disadvantage of these tomography techniques is that a large number of antennas needed to generate an image close enough to the actual material distribution of the target [11].

On the other hand, several studies have reported the classification of the raw microwave measurements without inversion. Saadat *et al.* implemented a biometric system that utilizes a single antenna (at close proximity) to identify an individual by targeting the wrist or triceps region [12]. This was tested on mobile and stationary subjects, achieving classification accuracies of 93% and 98%, respectively. Although the reported accuracies are somewhat high and the hardware setup is minimal, the sample scanning length required to achieve this is 30 seconds.

Diederichs *et al.* developed a hardware setup for individual identification by transmitting mm-waves through a user's hand [13]. The collected data (5 individuals) is classified using the random forest learning model, yielding over 80% in classification accuracy. Both previous techniques required physical contact between the sensor and the individual.

Xu *et al.* developed a Wi-Fi human identification system that can work through walls [14]. The system captures the Channel State Information (CSI) and uses the Time-Reversal (TR) method to extract features. Using 3 antenna pairs, an identification accuracy of 98.78% is achieved when identifying 11 individuals.

Liu *et al.* utilized CSI for individual authentication using Support Vector Machines (SVMs) [15]. Data was collected

[1]Ala-Addin Nabulsi, Waleed Al-Shaikhli , Clayton Kettlewell, Kyle Hejtmanek, Ahmed M. Hassan, and Reza Derakhshani are with the Department of Computer Science and Electrical Engineering, University of Missouri-Kansas City, Kansas City, MO 64110 USA (e-mail: angxb@mail.umkc.edu; waleed.al-shaikhli@mail.umkc.edu; ck7w2@mail.umkc.edu; kdh5zb@mail.umkc.edu; hassanam@umkc.edu; derakhshanir@umkc.edu).

in an office building and in an apartment, reportedly making the model more robust to environmental noise. Classification accuracies above 90% were achieved.

In this work, we explore scattered microwave signals, in the S-band, as an accurate non-contact biometric technique. Compared to previous biometric studies, a new microwave system is developed herein to allow the non-contact biometric classification. Using this system, we collected measurements from simple 3D printed targets as well as from the forearms of human volunteers. Moreover, we explored the classification accuracy of different machine learning techniques as the number of antennas is varied. Preliminary classification results of the measurements from simple targets were recently presented in our conference paper [16].

This paper is organized as follows. Section II presents the proposed methods and techniques which include data collection setup, collected datasets, data preprocessing, classification, and dimensionality reduction. Section III presents the experimental results and analysis and Section IV summarizes the Conclusions.

II. Methods

A. Data Collection Setup

The experimental hardware setup used to collect the microwave data is outlined in Fig. 1 to Fig.4. Inside the wooden container, is a circular antenna array consisting of 8 low-cost Pasternack PE51078 Rubber Duck, Reverse Polarity dipole antennas (typically employed in wireless routers) operating at 2.45 GHz, with a 5 dBi omni directional radiation pattern. The energy levels associated with this frequency range is very low (non-ionizing) and considered safe for humans [17]. The 8 antennas are connected to a two-port Agilent N5230C PNA-L Network Analyzer via a Mini-Circuits ZTVX-8-12-S DP8T switch network. During data collection, one antenna is transmitting while the rest are receiving, taking turns until the process is complete. The complex scattering parameters are recorded from each antenna pair, resulting in an 8x8 S-parameter matrix. Each collected sample is represented by a feature vector, of 128 values in length, which represents the magnitude and phase of the 64 S-parameters.

Fig. 5 shows the magnitude of one column of the scattering matrix, [S_{15}, S_{25}, S_{35}, S_{45}, S_{55}, S_{65}, S_{75}, S_{85}], experimentally measured with no target. Fig. 5 is a measure of the coupling between the antennas when Antenna 5 is transmitting, and all 8 antennas are receiving. Fig. 5 shows that, when Antenna 5 is transmitting, maximum coupling occurs to the two antennas on both sides of Antenna 5, which are Antenna 4 and Antenna 6, shown in Fig. 3. The coupling to these two antennas, S_{45} and S_{65}, is around -19 dB. Antennas at a further distance from Antenna 5 experience progressively lower coupling. Fig. 5 shows that the coupling between Antenna 5 and the other antennas ranges from -25 dB to -19 dB. Similar coupling patterns were achieved when antennas other than Antenna 5 were transmitting.

B. Dataset A: Foil-wrapped Tubes

For dataset A, 10 tubes of different cross-sectional shapes were covered by aluminum foil. Crescent, circle, L, cross, square, star, trefoil, triangle, T, and the pentagon cross-section shapes were used (Fig. 2 shows a top view of the samples). The dimensions of the samples and the antenna array are described in Table I, where "Antenna Array" refers to the circular antenna array and the Scan Area refers to the inner circumference in which the tubes' locations were confined. Each tube was placed in the data collection rig in 7 different configurations, namely: centered, 45-degree rotation, 90-degree rotation, shifted down, shifted left, shifted right, and shifted up, as seen in Fig. 3. For each configuration, 50 samples were collected, resulting in 350 samples per tube shape (class), yielding a total of 3,500 samples.

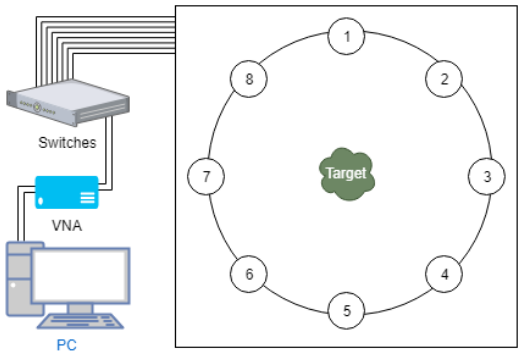

Fig. 1. Data Collection Setup: The VNA sends the signals, through the DP8T switch Network, to the antenna pairs. Next the PC logs the generated scatter data.

Fig. 2. Sample tube shapes used in dataset A: crescent, trefoil, pentagon, plus, circle, square, star, T, triangle, and L

C. Dataset B: Human Participants with Complete S-parameter Matrix

Dataset B was collected from 15 volunteers per a University of Missouri - Kansas City Institutional Review Board (IRB) protocol. During each session, the participants were asked to grip a handle placed in the middle of the antenna array so that their wrist and forearm would be positioned in the center of the 8 antennas (Fig 4). Then 5 samples were collected. The participants were then asked to retract their forearm and repeat the process 30 times, yielding 150 samples per subject and a total of 2,250 samples for dataset B.

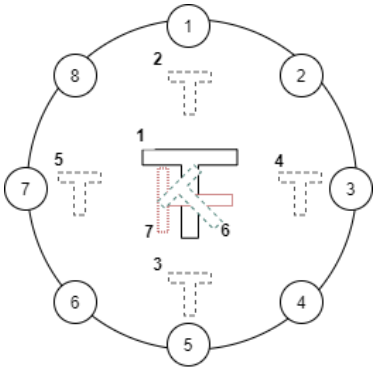

Fig. 3. The 7 configurations used for collecting the Tube data (Not to scale).

TABLE I
CROSS-SECTIONAL DIMENSIONS OF TUBE SAMPLES AND CIRCULAR ANTENNA ARRAY (IN CM).

No.	Shape	Side (cm)	Diameter (cm)
-	Antenna Array	-	40.5
-	Scan Area	-	14
1	Square	5	-
2	Star	5.5	4.68
3	T	8	-
4	Triangle	7	-
5	L	7.5	-
6	Crescent	-	8
7	Trefoil	6.5	3.75
8	Circle	-	6
9	Pentagon	5	4.25
10	Plus	-	8

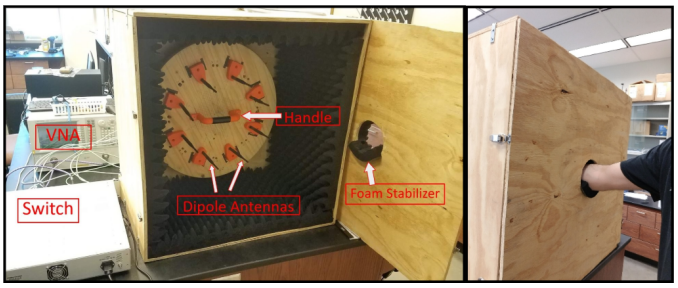

Fig. 4. Left: The interior of the microwave scanning system. Right: Closed scanning system with volunteer's forearm placed through the opening of the box to the center of the antenna array.

D. Dataset C: Human Participants with Incomplete S-parameter Matrix

Dataset C initially consisted of 34 volunteers collected similarly to Dataset B. However, the back-scatter (i.e. the diagonal of the scattering matrix) was not recorded for all 8 antennas. A total of 5,100 samples were collected in this dataset. Classification performance on this 34-subject data (without back-scatter) is also given and compared to the 15-subject data. The goal of Dataset C is to test the classification accuracy for the case of incomplete measurement of the S-parameter matrix which can be used to simplify future versions of the experimental setup [18].

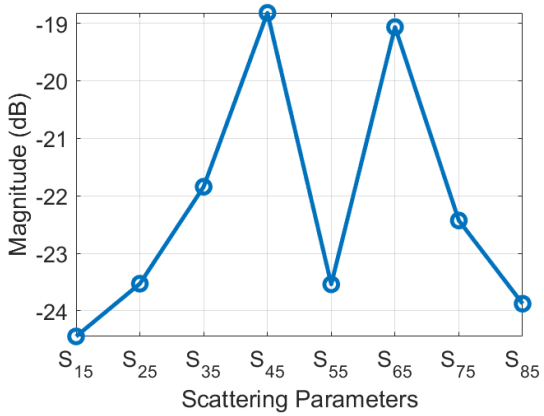

Fig. 5. Magnitude of the measured S-parameters when no target is resent in the experimental setup. For clarity only 8 of the 64 measured S-parameters in this case are shown.

E. Data Preprocessing

Each datapoint is in the form of a complex 8x8 S-parameter matrix. The data is then converted into Magnitude and Phase (degrees).

The dataset's phase components were normalized to [0, 1], since the phase can be up to two orders of magnitude larger than the magnitude in the dataset which would negatively affect the classifier training process. Finally, for each dataset, the corresponding class labels were generated for supervised training and evaluation of the resulting classifiers.

F. Classification

Fig. 6 shows examples of the measured S-parameters from the 10 foil-wrapped targets in Dataset A. Fig. 6a shows the magnitude of the S_{51} measurement and Fig. 6b shows the magnitude of S_{72} according to the antenna numbering shown in Fig. 3. For each target, 350 measurements are plotted to show the variance in the data with respect to the measurement repetition and the target orientation/location. Fig. 6a shows that the magnitude of S_{51} by itself is insufficient to classify the 10 targets because all targets show some level of overlap. However, combining the magnitude of S_{51} with the magnitude of S_{72} shows that Target 7 and Target 9 are distinguishable. Similarly, Target 2 and Target 5 are indistinguishable if only the magnitude of S_{72} is used by itself. However, the addition of the magnitude of S_{51} shows clear separation between the measurements from Target 2 and Target 5. Hence, increasing the number of antennas will expand the size of the S-parameters matrix for each target facilitating their accurate classification. Moreover, Fig. 6 shows the complexity of developing a decision-tree for the classification of such a large number of targets from such a large dataset. This complexity shows the clear need for the machine learning techniques described in the next subsections.

We chose two types of classifiers for this study: Naive Bayesian as a simple yet robust baseline, and Support Vector Machine as a more complex option capable of higher accuracy.

1) Naive Bayesian (NB)

This article has been accepted for publication in a future issue of this journal, but has not been fully edited. Content may change prior to final publication. Citation information: DOI 10.1109/OJAP.2020.2986001, IEEE Open Journal of Antennas and Propagation

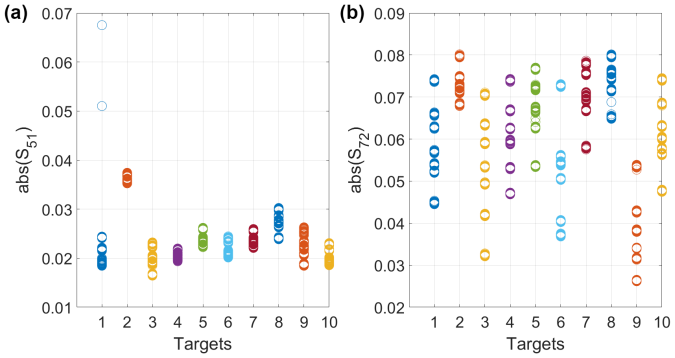

Fig. 6. Comparison of the S-parameter magnitude for the 10 targets in Dataset A: (a) Magnitude of S_{51} and (b) Magnitude of S_{72}.

The NB classifier utilizes Bayes' Rule to calculate the conditional probabilities of each class given the data present, assuming independence between input features. The trained classifier decides the incoming data labels based on the class with the highest probability [19].

2) Support Vector Machine (SVM)
SVM is a classifier that divides the input space into 2 classes by maximizing the hyperplane margins from the boundaries of the class samples in the training data in an intermediate space spanned by a set of kernels. Since the SVM is a binary classifier, multi-class problems usually utilized multiple classifiers using a one vs all scheme (i.e. class C vs not Class C) [20].

For each type of classifier, the following procedure is performed (Fig. 7):

- Test Holdout: The last 30% of the session data is held out for testing while the remaining 70% of the session data is used for cross-validation (CV).
- Monte-Carlo Shuffling: After the initial data division, the CV set is shuffled. This step, along with the following steps, are repeated 10 times.
- 4-fold Cross-Validation: The following is also repeated 4 times:
  - Training: 75% is used for training the classifier and the remaining 25% of the CV data is held out for validation. The same classifier is evaluated with data from the remaining shuffles and folds. The classifier hyperparameters were determined experimentally for each antenna set and dataset.
  - Validation: The trained classifier is then evaluated using the validation data. This process is repeated three more times until all the 4 CV partitions have participated both in training and validation.
- Evaluation: the classifier is evaluated using the test data.

This means that for each classifier type and antenna set, the aggregate results of 10x4 = 40 classifiers are reported.

G. Reduced Antenna Arrays

To study the effects of using fewer antennas, we repeated the classification process by taking signals from subsets of the antennas in the original array.

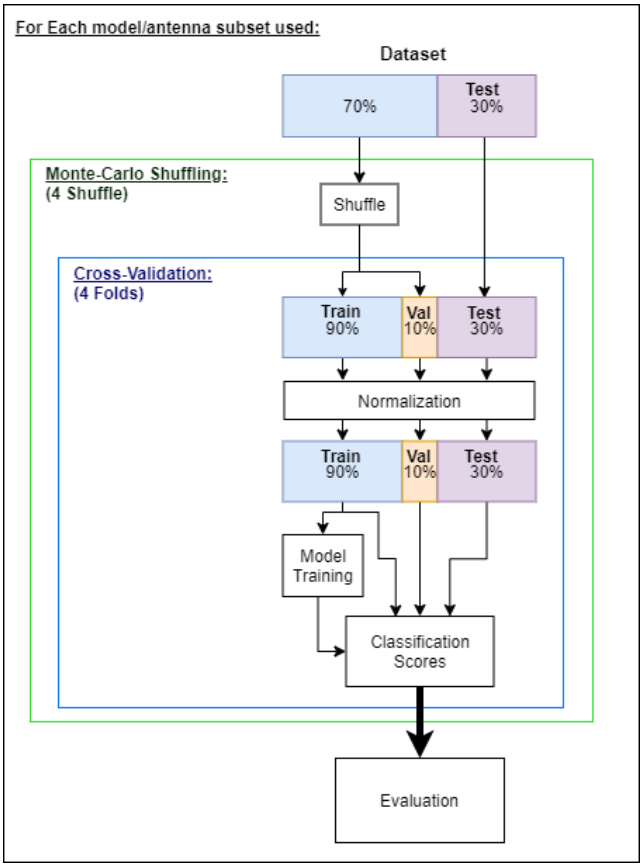

Fig. 7. Flowchart of classifier model building and evaluation (MB/E) used for each classifier type and/or antenna subset.

The process visualized in Fig. 7 is repeated for subsets of 4 and 2 antennas. For 4-antenna subsets, 2 datasets are generated using the corresponding rows and columns from the S-matrix (referred to as "4-atn" in section III). Antenna subset 4-atn (1) consisted of antennas [1, 3, 5, 7], while antenna subset 4-atn (2) consisted of antennas [2, 4, 6, 8], respectively. Similarly, 4 subsets of antenna pairs (referred to as "2-atn" in section III) were generated. Antenna subset 2-atn (1) consisted of antennas [1, 5], antenna subset 2-atn (2) consisted of antennas [2, 6], antenna subset 2-atn (3) consisted of antennas [3, 7], and antenna subset 2-atn (4) consisted of antennas [4, 8], respectively. As a result of reducing the number of antennas, the input dimensionality was reduced from 128 to 32 for 4-atn and to 8 for 2-atn, respectively.

The classification results for the full antenna set (8-atn), the two 4-atn subsets, and the four 2-atn subsets are reported in the following section.

III. Results and Discussion

We assessed our system's performance in terms of Area Under Curve (AUC), Equal Error Rate (EER), and decidability (d'). These classification metrics are widely used in biometrics, and are derived from the Receiver Operating Characteristic (ROC) curve and match score distributions [21], [22]. The AUC summarizes the classifier's performance across an aggregate of thresholds (the closer to 1 the better, with 0.5

denoting random decision making). The EER represents the classification error at a decision threshold where type I and II errors are equal. Type I error is also known as false positive (e.g. the false positive for User 1 will be the percentage of measurements from the other users that are mistakenly classified as User 1), and type II error is also referred to as false negative (e.g. the percentage of measurements from User 1 that are mistakenly classified as not belonging to User 1). The decidability (d') is derived from the distance between the means of the class distributions divided by the square-root of their average variances [23].

The data division schemes used can be seen in Fig. 8. Regarding division and stratification schemes for the human datasets B and C, the long-term data division refers to using a different session's data (with a meaningful time lapse or other factors causing similar intra-subject measurement variations) for training, validation, and testing; while the short-term data division refers to having each collection session's data divided among the training, validation, and testing sets (which entails smaller intra-sample variations). For the foil-wrapped tubes, the configuration-independent data division refers to using different configurations' data for training, validation, and testing.

The model classification performances are compared just using the EER metric for brevity, but all the above metrics are presented in the results tables for completeness.

A. Foil Tubes

Configuration-independent Division: Table II (and Fig. 9) shows that the SVM classifier, with a linear kernel (used in all SMV classifiers in this work), yielded a testing EER of 19.48% for the 8-antenna set. The testing EER increased for the first 4-antenna subset to 24.51%, while remaining fairly constant at 19.15% for the second 4-antenna subset. The 2 antenna subsets achieved testing EERs of 24.15%, 21.88%, 32.47%, and 24.89%. The NB classifier yielded a 20.76% testing EER for the 8-antenna set. For the first and second 4-antenna subsets, the NB showed a testing EER of 41.08% and 42.08%, respectively. The first and third 2-antenna subsets yielded testing EERs of 47.0% and 28.28%, respectively. The second and fourth 2-antenna subsets each yielded testing EERs of 36.67% and 36.65%, respectively.

B. Human Forearms (15 subjects)

Long-term Division: Table III (and Fig. 10) shows that the SVM model performed very well on the human data, yielding a testing EER of just 1.03% for the 8-antenna set. The testing EERs increased slightly for the first 4-antenna subset (1.43%), while decreasing slightly to 0.99% for the second subset. The four 2-antenna subsets showed more variations in performance, with testing EERs ranging from 4.48% to 8.58%. As for the NB classifier, it yielded a higher testing EER of 1.86% for the 8-antenna set. The testing EER increased to 4.9-9.91% for the 4-antenna subsets, while the four 2-antenna subsets yielded testing EERs in the range of 1.45-4.97%.

Short-term Division: Table IV (and Fig. 11) shows that the SVM model also performed very well on the human data, with a testing EER of 0.22% for the 8-antenna set. The testing EER for both 4 antenna subsets decreased to 0% and 0.02%, respectively. The testing EERs increased once more, for the four 2-antenna subsets, to 2.5-4.65%. As for the NB classifier, it yielded a testing EER of 0.11% for the 8-antenna set, while the error increased slightly for one of the 4-antenna subsets to 0.13%. However, the EER decreased for the second antenna subset to 0%. The four 2-antenna subsets yielded testing EERs in the range of 0.8 to 1.98%.

C. Human Forearms (34 subjects)

Long-term Division: Table V (and Fig. 12) shows that the SVM and NB classifiers yielded testing EERs of 2.18% and 6.38%, respectively using the 8-antenna set (excluding the back-scatter data).

Short-term Division: Table V (and Fig. 12) shows that the SVM model yielded a lower testing EER of 0.26% using the 8-antenna set (excluding the back-scatter data) and a testing EER of 0.1% for the NB model.

Overall, for the human forearms classification, it is observed that the SVM and NB classifiers achieve promising results using the 8-antenna set, the 4-antenna subsets, and for some of the 2-antenna subsets. The short-term data division outperforms the long-term division (as expected), but both show promise noting that the long-term data division is more germane to real world biometric use cases. All models showed an overall increase in error as the number of antennas decrease, with the exception of the 4-antenna subsets for long-term division of the NB classifier. This anomaly maybe due to high inter-variable dependencies for that case, which the NB model does not take into account. On the other hand, these results predict that increasing the number of antennas, more than 8, has the potential to further reduce the error reported for the 8-antenna configuration.

In case of the tubes, the classifiers that used the configuration-independent division scheme were able to classify (albeit with less accuracy) tube shapes in new configurations that they hadn't seen before. Changing the tube shapes in the full 8-antenna set had more of an effect on the SVM test results (with EERs ranging from 10 to 20%) while less of an effect on the NB results (18-20% for testing EER).

Needless to say, collecting more data from the target (i.e. the tubes or the human volunteers) with different configurations is likely to lead to better results and insights, although at the cost of a longer training period.

IV. Conclusion

In this work, microwave signals collected from foil tubes and human forearms were classified using multiple methods and different antenna set combinations. The classification results show promise for the use of microwave signals for biometric authentication. The relatively low drop in classification accuracy with reductions in antenna set sizes for human subjects' data suggests the possibility of utilizing systems with fewer antennas, leading to reduced hardware costs and computational complexity. Further analysis and testing is required to better evaluate and eventually improve this system. Future

This article has been accepted for publication in a future issue of this journal, but has not been fully edited. Content may change prior to final publication. Citation information: DOI 10.1109/OJAP.2020.2986001, IEEE Open Journal of Antennas and Propagation

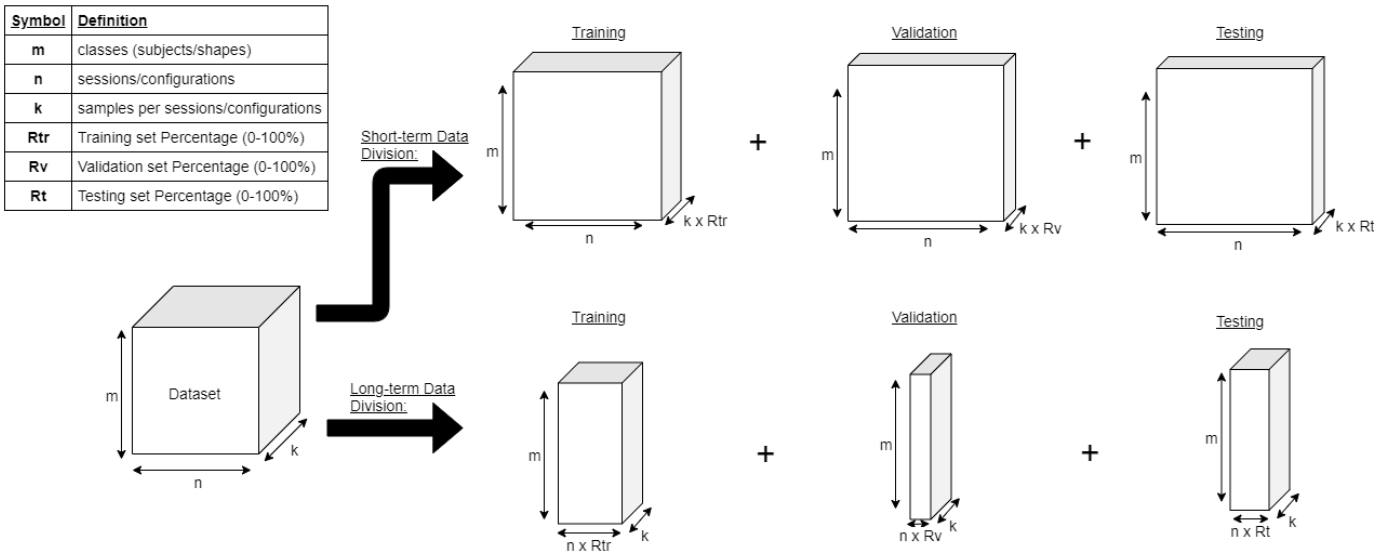

Fig. 8. Explaining different type of data divisions used: Short-term data division (referred to as configuration dependent for foil-wrapped tubes) and Long-term data division (referred to as configuration independent for foil-wrapped tubes).

TABLE II
CLASSIFICATION RESULTS FROM FOIL TUBES WITH CONFIGURATION-INDEPENDENT DATA DIVISION SCHEME.

		8-atn		4-atn (1)		4-atn (2)		2-atn (1)		2-atn (2)		2-atn (3)		2-atn (4)	
		Val	Test	Val	Test	Val	Test	Val	Test	Val	Test	Val	Test	Val	Test
SVM	**AUC**	0.9	0.87	0.82	0.83	0.88	0.89	0.76	0.85	0.79	0.85	0.78	0.74	0.81	0.83
	EER(%)	16.4	19.48	24.98	24.51	20.44	19.15	29.92	24.15	27.23	21.88	29.77	32.47	27.86	24.89
	D'	1.77	1.48	1.11	1.13	1.43	1.58	0.8	1.1	0.93	1.17	0.77	0.76	0.92	1.06
NB	**AUC**	0.88	0.81	0.65	0.65	0.73	0.62	0.58	0.56	0.67	0.68	0.8	0.76	0.63	0.71
	EER(%)	17.5	20.76	40.64	41.08	33.64	42.08	45.66	47.0	39.08	36.67	21.81	28.28	41.65	36.65
	D'	1.74	1.11	0.65	0.66	0.96	0.54	0.45	0.36	0.67	0.78	0.93	1.19	0.6	0.87

TABLE III
CLASSIFICATION RESULTS FROM HUMAN FOREARMS WITH LONG-TERM DATA DIVISION SCHEME.

		8-atn		4-atn (1)		4-atn (2)		2-atn (1)		2-atn (2)		2-atn (3)		2-atn (4)	
		Val	Test	Val	Test	Val	Test	Val	Test	Val	Test	Val	Test	Val	Test
SVM	**AUC**	0.99	1.00	0.99	1.00	1.00	1.00	0.97	0.99	0.98	0.99	0.95	0.97	0.98	0.97
	EER(%)	5.55	1.03	1.09	1.43	0.92	0.99	8.11	4.99	5.52	4.48	13.39	8.58	6.34	8.31
	D'	2.1	3.37	1.9	2.15	1.78	1.96	1.55	1.93	1.48	1.61	1.57	1.87	1.63	1.64
NB	**AUC**	1.00	1.00	0.98	0.99	0.98	0.97	0.98	0.99	0.99	0.99	0.98	0.98	0.98	0.97
	EER(%)	1.19	1.86	4.4	4.9	8.67	9.91	3.14	2.42	1.72	1.45	2.65	3.52	2.82	4.97
	D'	9.06	6.7	4.52	4.26	3.25	2.98	3.89	4.12	6.04	6.71	4.8	4.07	5.24	3.67

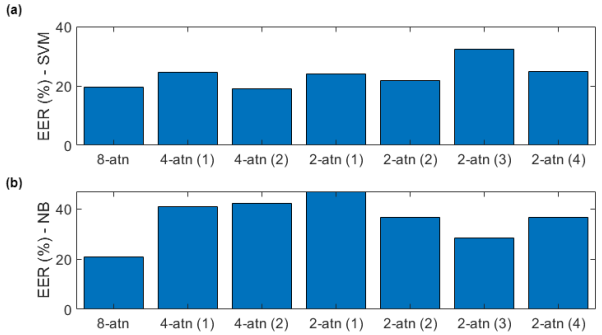

Fig. 9. Classification results from Foil Tubes with Configuration-independent data division scheme: Testing EERs for (a) the SVM classifier and (b) the NB classifier.

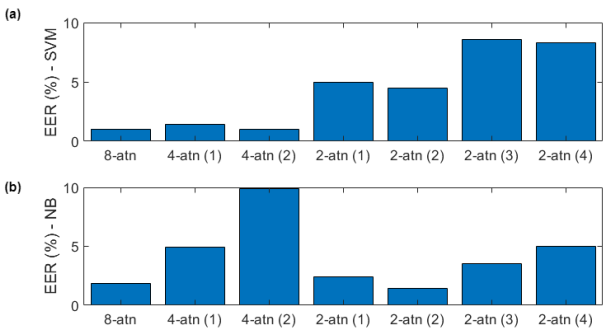

Fig. 10. Classification results from Human Forearms with Long-term data division scheme: Testing EERs for (a) the SVM classifier and (b) the NB classifier.

This article has been accepted for publication in a future issue of this journal, but has not been fully edited. Content may change prior to final publication. Citation information: DOI 10.1109/OJAP.2020.2986001, IEEE Open Journal of Antennas and Propagation

TABLE IV
CLASSIFICATION RESULTS FROM HUMAN FOREARMS WITH SHORT-TERM DATA DIVISION SCHEME.

		8-atn		4-atn (1)		4-atn (2)		2-atn (1)		2-atn (2)		2-atn (3)		2-atn (4)	
		Val	Test	Val	Test	Val	Test	Val	Test	Val	Test	Val	Test	Val	Test
SVM	AUC	1.00	1.00	1.00	1.00	1.00	1.00	0.99	0.99	0.99	0.99	0.99	0.99	0.99	0.99
	EER(%)	0.04	0.22	0.00	0.00	0.04	0.02	4.62	4.65	2.83	2.5	3.37	3.6	4.75	4.18
	D'	3.07	3.04	2.22	2.22	2.59	2.59	2.1	2.12	1.35	1.36	1.89	1.89	1.77	1.87
NB	AUC	1.00	1.00	1.00	1.00	1.00	1.00	0.99	1.00	1.00	1.00	1.00	0.99	1.00	1.00
	EER(%)	0.14	0.11	0.06	0.13	0.06	0.00	1.86	1.98	0.73	0.8	1.5	1.55	1.59	1.55
	D'	28.64	32.0	30.06	29.1	45.31	3198.45	4.82	4.93	7.75	8.02	6.43	6.27	6.2	6.1

TABLE V
CLASSIFICATION RESULTS FROM HUMAN FOREARMS OF 34 SUBJECTS (EXCLUDING BACK-SCATTER)

		Long-term		Short-term	
		Val	Test	Val	Test
SVM	AUC	0.99	0.99	1.00	1.00
	EER(%)	2.04	2.18	0.03	0.26
	D'	1.21	1.33	1.2	1.19
NB	AUC	0.97	0.95	1.00	1.00
	EER(%)	4.55	6.38	0.06	0.1
	D'	3.89	2.96	41.2	32.12

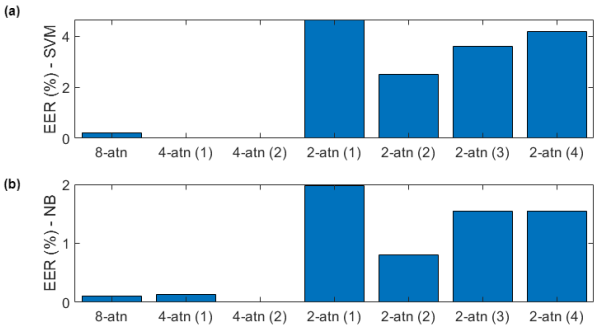

Fig. 11. Classification results from Human Forearms with Short-term data division scheme: Testing EERs for (a) the SVM classifier and (b) the NB classifier.

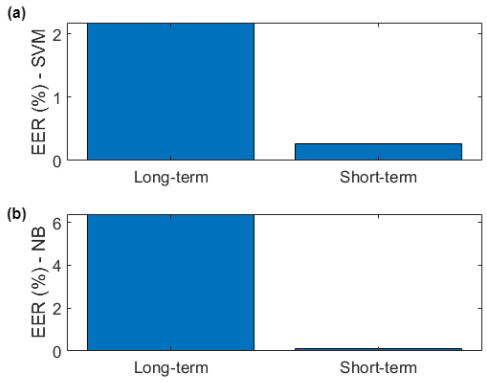

Fig. 12. Classification results from Human Forearms of 34 subjects (excluding backs scatter): Testing EERs for (a) the SVM classifier and (b) the NB classifier.

work includes collecting larger datasets to allow for training more capable models and statistically significant results. Exploring more directive antennas and multiple frequencies will also be pursued to further increase the classification accuracy. Classification-oriented subspace projections such as Fisher linear discriminant analysis for better dimensionality reduction and reducing the number of antennas to make the system more economical are also among other suggested next steps.

V. ACKNOWLEDGEMENT

The authors would like to thank George Scott, Blake Willig, Caylin Hartshorn, and Somen Baidya (University of Missouri-Kansas City) for their assisting efforts in developing the data collection setup and collecting the data used in this work.

REFERENCES

[1] L. O'Gorman, "An overview of fingerprint verification technologies," *Information Security Technical Report*, vol. 3, no. 1, pp. 21–32, 1998.
[2] L. Masek *et al.*, "Recognition of human iris patterns for biometric identification," Ph.D. dissertation, Master's thesis, University of Western Australia, 2003.
[3] K. I. Chang, K. W. Bowyer, and P. J. Flynn, "An evaluation of multimodal 2d+ 3d face biometrics," *IEEE transactions on pattern analysis and machine intelligence*, vol. 27, no. 4, pp. 619–624, 2005.
[4] R. Derakhshani and A. Ross, "A texture-based neural network classifier for biometric identification using ocular surface vasculature," in *2007 International Joint Conference on Neural Networks*. IEEE, 2007, pp. 2982–2987.
[5] J. Yang, D. Zhang, J.-y. Yang, and B. Niu, "Globally maximizing, locally minimizing: unsupervised discriminant projection with applications to face and palm biometrics," *IEEE transactions on pattern analysis and machine intelligence*, vol. 29, no. 4, pp. 650–664, 2007.
[6] G. Ariyanto and M. S. Nixon, "Model-based 3d gait biometrics," in *2011 International Joint Conference on Biometrics (IJCB)*. IEEE, 2011, pp. 1–7.
[7] K. Delac and M. Grgic, "A survey of biometric recognition methods," in *Proceedings. Elmar-2004. 46th International Symposium on Electronics in Marine*. IEEE, 2004, pp. 184–193.
[8] A. Rattani, N. Poh, and A. Ross, "Analysis of user-specific score characteristics for spoof biometric attacks," in *2012 IEEE Computer Society Conference on Computer Vision and Pattern Recognition Workshops*. IEEE, 2012, pp. 124–129.
[9] M. Ostadrahimi, P. Mojabi, S. Noghanian, L. Shafai, S. Pistorius, and J. LoVetri, "A novel microwave tomography system based on the scattering probe technique," *IEEE Transactions on instrumentation and measurement*, vol. 61, no. 2, pp. 379–390, 2012.
[10] Y. A. Rahama, O. Al Aryani, U. A. Din, M. Al Awar, A. Zakaria, and N. Qaddoumi, "Novel microwave tomography system using a phased-array antenna," *IEEE Transactions on Microwave Theory and Techniques*, vol. 66, no. 11, pp. 5119–5128, 2018.
[11] C. Gilmore, A. Zakaria, S. Pistorius, and J. LoVetri, "Microwave imaging of human forearms: Pilot study and image enhancement," *Journal of Biomedical Imaging*, vol. 2013, p. 19, 2013.
[12] W. Saadat, S. A. Raurale, G. A. Conway, and J. McAllister, "Physical layer biometrics using antennas for secure wearable wireless communication," *IEEE Transactions on Antennas and Propagation*, 2018.

[13] K. Diederichs, A. Qiu, and G. Shaker, "Wireless biometric individual identification utilizing millimeter waves," *IEEE Sensors Letters*, vol. 1, no. 1, pp. 1–4, 2017.

[14] Q. Xu, Y. Chen, B. Wang, and K. R. Liu, "Radio biometrics: Human recognition through a wall," *IEEE Transactions on Information Forensics and Security*, vol. 12, no. 5, pp. 1141–1155, 2017.

[15] H. Liu, Y. Wang, J. Liu, J. Yang, and Y. Chen, "Practical user authentication leveraging channel state information (csi)," in *Proceedings of the 9th ACM symposium on Information, computer and communications security*. ACM, 2014, pp. 389–400.

[16] C. Kettlewell, K. Hetjmanek, G. Scott, W. Al-Shaikhli, B. Willig, A.-A. Nabulsi, S. Baidya, R. Derakhshani, and A. M. Hassan, "Experimental microwave target identification using machine learning," in *2019 IEEE International Symposium on Antennas and Propagation and USNC-URSI Radio Science Meeting*. IEEE, 2019, pp. 227–228.

[17] E. Fields, R. F. Cleveland, and J. L. Ulcek, "Questions and answers about biological effects and potential hazards of radiofrequency electromagnetic fields," in *Oet Bulletin*. Citeseer, 1999.

[18] A. E. Stancombe, K. S. Bialkowski, and A. M. Abbosh, "Portable microwave head imaging system using software-defined radio and switching network," *IEEE Journal of Electromagnetics, RF and Microwaves in Medicine and Biology*, vol. 3, no. 4, pp. 284–291, 2019.

[19] P. Langley, W. Iba, K. Thompson *et al.*, "An analysis of bayesian classifiers," in *Aaai*, vol. 90, 1992, pp. 223–228.

[20] J. Weston and C. Watkins, "Multi-class support vector machines," Citeseer, Tech. Rep., 1998.

[21] S. P. Tankasala, P. Doynov, R. R. Derakhshani, A. Ross, and S. Crihalmeanu, "Biometric recognition of conjunctival vasculature using glcm features," in *2011 International Conference on Image Information Processing*. IEEE, 2011, pp. 1–6.

[22] M. Xia, J. Ma, J. Li, Y. Liu, Y. Zeng, and Z. Nie, "Gradient and svm based biometric identification using human body communication," in *2016 IEEE International Conference of Online Analysis and Computing Science (ICOACS)*, 2016, pp. 61–65.

[23] N. Macmillan and C. Douglas, "Detection theory: a user's guide/neil a," 2005.